Available online at www.sciencedirect.com
SCIENCE DIRECT
Journal of Molecular Spectroscopy 236 (2006) 58–69
Journal of MOLECULAR SPECTROSCOPY
www.elsevier.com/locate/jms

High sensitivity absorption spectroscopy of HDO by ICLAS-VeCSEL between 9100 and 9640 cm^{-1}

Olga Naumenko [a], Olga Leshchishina [a], Alain Campargue [b,*]

[a] *Institute of Atmospheric Optics, Russian Academy of Sciences, Tomsk, 634055, Russia*
[b] *Laboratoire de Spectrométrie Physique (associated with CNRS, UMR 5588) Université Joseph Fourier de Grenoble, B.P. 87, 38402 Saint-Martin-d'Hères, Cedex, France*

Received 7 December 2005; in revised form 22 December 2005
Available online 7 February 2006

Abstract

The absorption spectrum of monodeuterated water has been recorded between 9100 and 9640 cm^{-1} using intracavity laser absorption spectroscopy (ICLAS) based on a vertical external cavity system emitting laser (VeCSEL). Overall 1706 lines were attributed to the HDO species. The spectrum assignment was performed on the basis of the ab initio calculations by Schwenke and Partridge. A set of 746 energy levels was derived from transitions assigned to 13 upper vibrational states, 300 of them being reported for the first time. Resonance interactions leading to an important strengthening and observations of the very weak $7\nu_2$ and $\nu_1 + 5\nu_2$ bands are discussed. A detailed line list has been generated.

Keywords: Water; ICLAS; Intracavity laser absorption spectroscopy; HDO; Rovibrational spectroscopy

1. Introduction

This contribution is part of our investigation of the HDO absorption spectrum by intracavity laser absorption spectroscopy (ICLAS) in the visible and near infrared ranges [1–6]. It is devoted to the 9100–9640 cm^{-1} region which extends to lower energy our previous studies. A review (up to 2003) of the absorption bands of HDO recorded between 9600 and 18 350 cm^{-1} by using different ICLAS spectrometers (Vertical External Cavity Surface Emitting Lasers, Ti: Sapphire, dyes) is presented in Fig. 1 of [6]. Since then, the analysis of the absorption spectrum of HDO above 9000 cm^{-1} has been extended by a few additional contributions:

- the FTS study of the 8900–9600 cm^{-1} [7] and 10 110–12 215 cm^{-1} [8] regions, obtained with a 123-m path length.
- the full coverage of the FTS absorption spectrum between 11 500 and 23 000 cm^{-1}, recorded with a 600-m path length [9].
- our recent high sensitivity ICLAS-Ti: Sapphire study of the 11 645–12 330 cm^{-1} region [10] which improved by more than one order of magnitude the FTS detection limit of [8,9] and then allowed to observe numerous weak lines.

The presently investigated spectral region (9100–9640 cm^{-1}) is shown in Fig. 1: it corresponds to a "transparency window" for both the main isotopologue, $H_2{}^{16}O$, and HDO. It lies between the much stronger $\nu_2 + 2\nu_3$ and $3\nu_3$ bands of HDO at 8611.095 and 10631.683 cm^{-1}, respectively (we use the traditional labeling of the vibrational modes: ν_1(2723.68 cm^{-1}), ν_2(1403.48 cm^{-1}), and ν_3(3707.47 cm^{-1}) for the OD stretching, the bending and the OH stretching vibration, respectively). The 9160–9390 cm^{-1} section was recorded in 1982 by ICLAS with an absorption sensitivity of 10^{-7} cm^{-1} using an Nd glass laser [11]. However, the limited tuning range of the Nd glass laser prevents a wider spectral

* Corresponding author. Fax: +33 4 76 63 54 95.
E-mail address: Alain.Campargue@ujf-grenoble.fr (A. Campargue).

0022-2852/$ - see front matter © 2006 Elsevier Inc. All rights reserved.
doi:10.1016/j.jms.2005.12.008

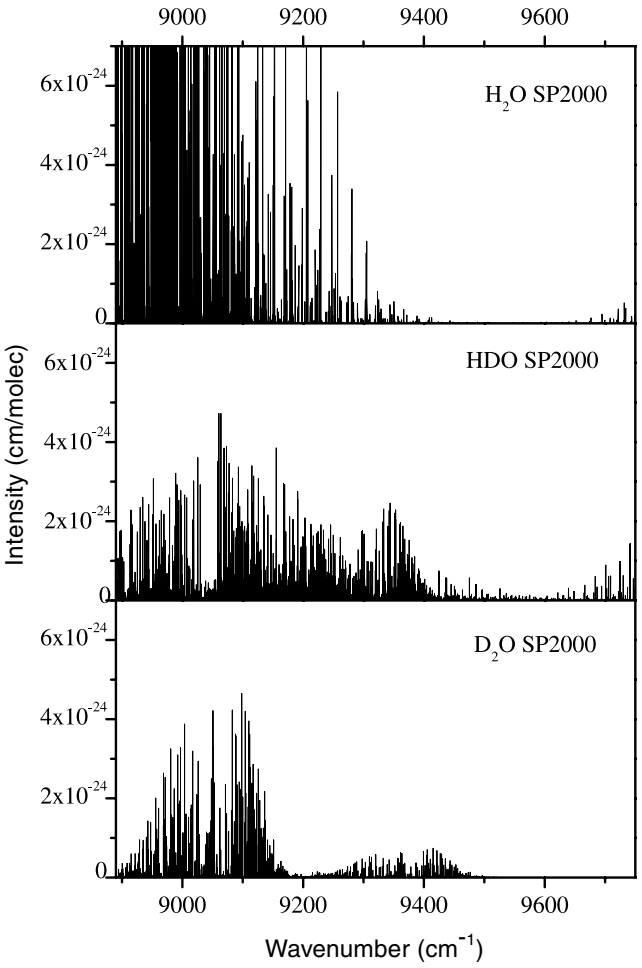

Fig. 1. Overview of the H_2O, HDO, and D_2O spectrum as calculated by Schwenke and Partridge (SP) [21,22]. Note that the intensity scale correspond to the pure species.

coverage and the achieved sensitivity and spectral resolution were not very good. As just mentioned, the analysis of the 8900–9600 cm^{-1} region was recently improved on the basis of a FTS absorption spectrum recorded with a 123-m path length and a 0.02 cm^{-1} resolution [7] but the high sensitivity of the ICLAS technique is expected to provide a much deeper knowledge of this spectral region.

2. Experimental procedure

2.1. The ICLAS-VeCSEL spectrometer

The ICLAS spectra were recorded with the experimental setup based on a VeCSEL previously described in [12,13]. Shortly, an undoped semiconductor QW 1/2 VCSEL structure, composed of quantum wells (QW) deposit over a high reflective Bragg mirror, is used as amplification medium in an external cavity where the cell is inserted. The emission wavelength can be tuned continuously by changing the temperature or the pump power of the active structure or simply by translating the structure perpendicularly to the laser and taking advantage of the non-uniformity of the radial growth. Using different VeCSEL structures, a full coverage of the 1.0–1.1 μm region was achieved. Such solid state spectrometers pumped by a commercial low cost low power 800 nm diode laser, are compact and provide sensitivity as low as $\alpha_{min} = 10^{-10} cm^{-1}$ or $3 \times 10^{-11} cm^{-1}/\sqrt{Hz}$ [12]. They were successfully applied in the 8800–10 100 cm^{-1} region for systematic investigations of the overtone spectra of molecules such as N_2O [13–15], CO_2 [16], H_2S [17], and H_2O [18]. The present report extends to lower energy a previous ICLAS-VeCSEL study of HDO between 9625 and 10 100 cm^{-1} [6]. The achieved sensitivity was on the order of $\alpha_{min} \sim 5 \times 10^{-9}$ cm^{-1}, which is not as good as the performances achieved at higher energy as a consequence of the poorer laser properties of the VeCSEL presently used. Note that depending on the materials (GaAs, InP, and GaSb), different types of 1/2 VeCSEL structures can be processed to give access to the 0.8–2.5 μm wavelength range at room temperature and in CW operation. For instance, we have recently demonstrated ICLAS-VeCSEL operating around 2.3 μm [19].

The spectra were recorded with generation times up to 130 μs, leading to equivalent absorption path lengths on the order of 23.4 km as the filling ratio of the laser cavity by the absorption cell was 60%. The spectral resolution was about 0.04 cm^{-1} slightly larger than the Döppler broadening (0.028 cm^{-1} FWHM). The cell was filled with a 1:1 mixture of H_2O and D_2O at a total pressure of about 18 hPa to obtain a mixture of H_2O:HDO:D_2O in a proportion close to 1:2:1. In the regions corresponding to the most intense absorption lines, additional spectra were recorded at lower pressures down to 1 hPa. Fig. 2 illustrates that the gain in terms of sensitivity achieved by ICLAS is more than one order of magnitude compared to FTS [7].

2.2. Line list construction

The wavenumber calibration procedure of the ICLAS recordings requires the knowledge of several reference line positions, for each 12 cm^{-1} wide section of the spectrum recorded by the 3754 photodiode array placed at the exit of the spectrograph. As often as possible, we used the HDO line positions measured by FTS [7] as reference. From the comparison of the wavenumber values obtained using independent reference lines, the accuracy of the ICLAS line positions was estimated to be around 0.002 cm^{-1} for well isolated line of intermediate intensity.

An important concern is the retrieval of line intensities: contrary to ICLAS based on dye or Ti:Sapphire lasers, the specific laser dynamics of VeCSELs prevents its systematic use for absolute quantitative measurements from ICLAS-VeCSEL spectra. For instance, our recent study [20] has showed, that in some experimental conditions (high pumping rate, very long generation times, high line intensity etc.) the absorption profile of the stronger lines can be strongly asymmetric in the ICLAS-VeCSEL spectrum and in some extreme conditions, replaced by *emission* (!) lines. These

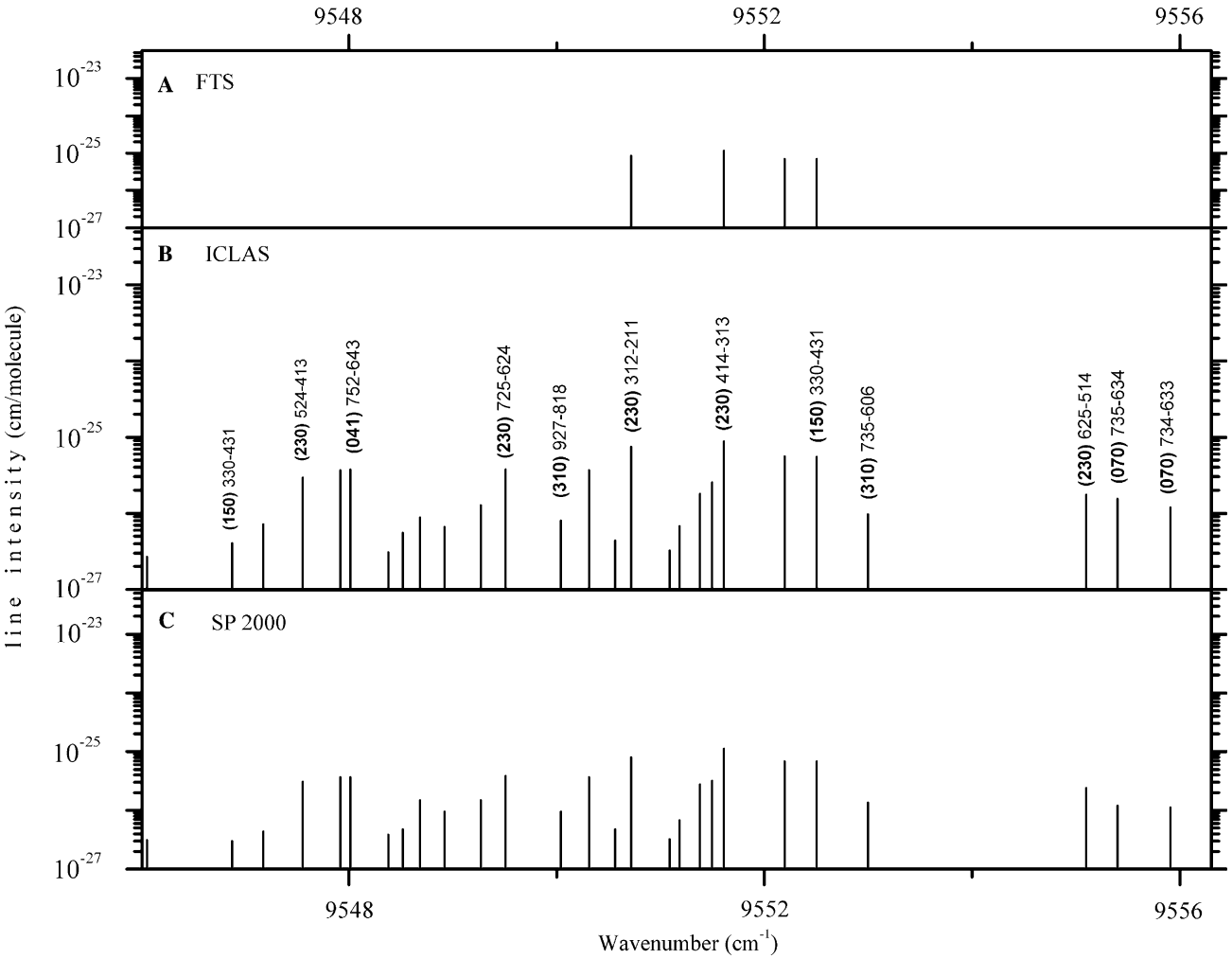

Fig. 2. Comparison of the HDO stick spectrum near 9552 cm^{-1} (A) retrieved from the FTS spectrum of [7], (B) retrieved from the ICLAS spectrum, and (C) calculated by Schwenke and Partridge [21,22]. The $(v'_1, v'_2, v'_3)J'K'_aK'_c - J''_aK''_aK''_c$ rotational assignments are given for part of the lines (the whole assignments are listed in the Supplementary material).

spectacular effects of *spectral condensation* have been characterized in [20] but are not fully understood.

In the present recordings, we took much care of choosing experimental conditions leading to symmetric line profile but even in such conditions, relative intensities are not trustable. This is illustrated for instance in Fig. 3 which shows that the absorption line intensity depends on the location of the line relative to the centre frequency of the VeCSEL emission profile. The comparison with the FTS spectrum of [7] indicates that the absorption is systematically underestimated when the line appears on the wing of the emission profile. In such circumstances, it was not reasonable to try to retrieve accurate line intensities from our spectra. However, the complete assignment of the spectrum relies greatly on the intensity criterion i.e., the reasonable matching between observed and calculated [21,22] intensities. Indeed, the quality of the calculated intensity values was tested in many different spectral regions and was found, in most cases, close to the experimental accuracy. Thus, certain efforts were undertaken to scale the experimental intensities against the calculated values.

Our main interest was the assignment of middle intensity and weak lines, since strong lines were previously analysed [7]. The scaling procedure was carried out in several steps. First, the observed intensities were roughly normalized against calculated values using the FTS identification list [7]. Then new assignments were performed for lines included in combination differences (CD) relations. The resulting identification list was subjected to a new scaling which involved, especially, the weakest lines. The scaling factors were chosen differently for different intensity range. Finally these factors were used for scaling the whole line list including a large number of still unassigned lines. As a result, a satisfactory agreement with the calculation was achieved for middle and weak lines (see Fig. 4) while the situation was less satisfactory for the strongest lines which where frequently saturated on the ICLAS spectra. The obtained intensity values proved to be of great help for the identification of the weakest lines not included into CD relations,

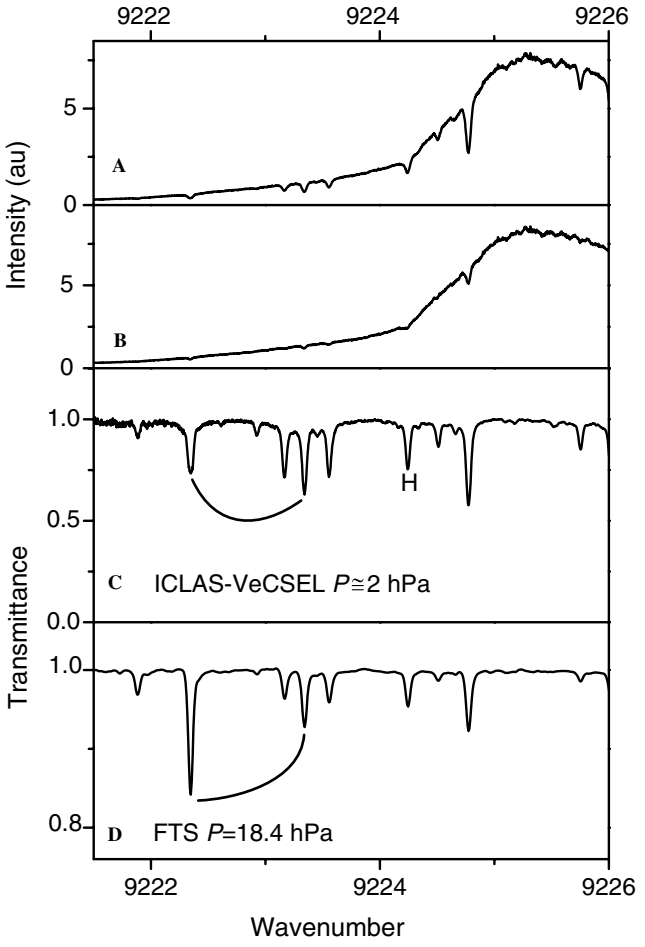

Fig. 3. Illustration of the recording procedure and of the distortion of the line intensities in the ICLAS-VeCSEL spectrum of HDO near 9224 cm^{-1}. The two upper panels present the ICLAS-VeCSEL spectra obtained with a generation time of 110 μs: (A) D_2O:HDO:H_2O mixture spectrum recorded at a pressure of about 2 hPa superimposed to the laser emission profile (B) laser emission background obtained with an empty cell. The ratio of the first spectrum by the second one gives the spectrum displayed in (C). The lower panel (D) presents for comparison the FTS spectrum of [7] obtained with an 18.4 hPa pressure. The comparison of the relative intensities of the lines displayed in C and D clearly shows that they are systematically underestimated by ICLAS-VeCSEL when the line centre is situated far from the maximum of the VeCSEL emission.

and in the case of blended lines. The weakest lines which have been detected have an intensity value on the order of 10^{-27} cm/mol.

3. Rovibrational assignments

The obtained line list includes a total of 2250 transitions corresponding to the superposition of the HDO, H_2O, and D_2O contributions. 195 H_2 ^{16}O lines were identified on the basis of the line list attached to [23] while 349 D_2O lines were discriminated by comparison with the ICLAS-VeCSEL D_2O spectrum recorded in the same region [24].

As stated in [7], the line positions calculated by Schwenke and Partridge [21,22] coincide with the experimental ones within 0.05 cm^{-1} on average, which, combined with the intensity matching, facilitated the assignment process. The rovibrational assignments were assessed by taking in consideration both CD relations and the fact that the (obs. − calc.) deviations of the energy levels depend smoothly on the J and K_a rotational quantum numbers. This is illustrated for instance in Fig. 5 for the $K_a = 0$–5 levels of the different investigated vibrational states. However, as we proceeded with our assignments, both theoretical predictions and experimental accuracy degraded for the weakest lines corresponding to the highly excited transitions that resulted in less reliable assignments, in particular, in the case of single line not involved in lower sate combination relations. Tentative assignments as well as lines blended by H_2O or D_2O lines are marked in the HDO identification list which is attached as Supplementary material. This list counts 2002 HDO transitions corresponding to 1706 absorption lines, some of them being unresolved blends while about 930 HDO transitions were reported in Ref. [7] in the 8713–9592 cm^{-1} spectral region, 718 of them falling into our region. Though we tried to assign all HDO lines predicted with sufficient intensity for observation, some could not be identified and included into the final list since they were superimposed to much stronger line. Only four lines are left unassigned.

The upper level energies were derived by adding the lower energy values [25] to the observed transitions. A total of 746 energy levels belonging to 13 vibrational states were obtained (see Table 1). 356, 87, and 3 of them were previously determined in [7], [6], and [8],respectively, yielding 300 newly derived energy levels. The state by state comparison with the results of [7] is included in Table 1. As expected, most of the new energy levels were obtained for the highly excited (041), (150), (230), and (070) states corresponding to the weakest bands. We could also reach higher J and K_a values for the three strongest bands, namely (201)–(000), (121)–(000), and (310)–(000). From the (obs. − calc.) extrapolation for energy levels with $K_a = 0$, we estimate at 9032.11 ± 0.1 and 9086.32 ± 0.05 cm^{-1}, the origin of the (041)–(000) and (070)–(000) bands, respectively (see Fig. 5).

Our energy levels listed in Tables 2 and 3 agree with that of [7] within 0.0036 cm^{-1} on average with a largest discrepancy of 0.026 cm^{-1} for the (230) [321] level at 9596.5320 cm^{-1}. We believe that in many cases our energy levels values are more precise since they are often derived from a larger number of lines reaching the same upper level and that, our program for automatic spectrum assignment allows for discarding the less accurate line positions among all the lines included into CD relations. In particular, our value for the above (230) [321] level is more accurate since it was derived from the CD of four lines with an rms error of 0.0024 cm^{-1} (see Table 3), while in [7] this level was obtained from a single line at 9441.1693 cm^{-1} which is blended by a two times stronger transition: (230) [313]–[414] (see Supplementary material). As mentioned above, our rovibrational assignment relied on the results of the global variational calculations

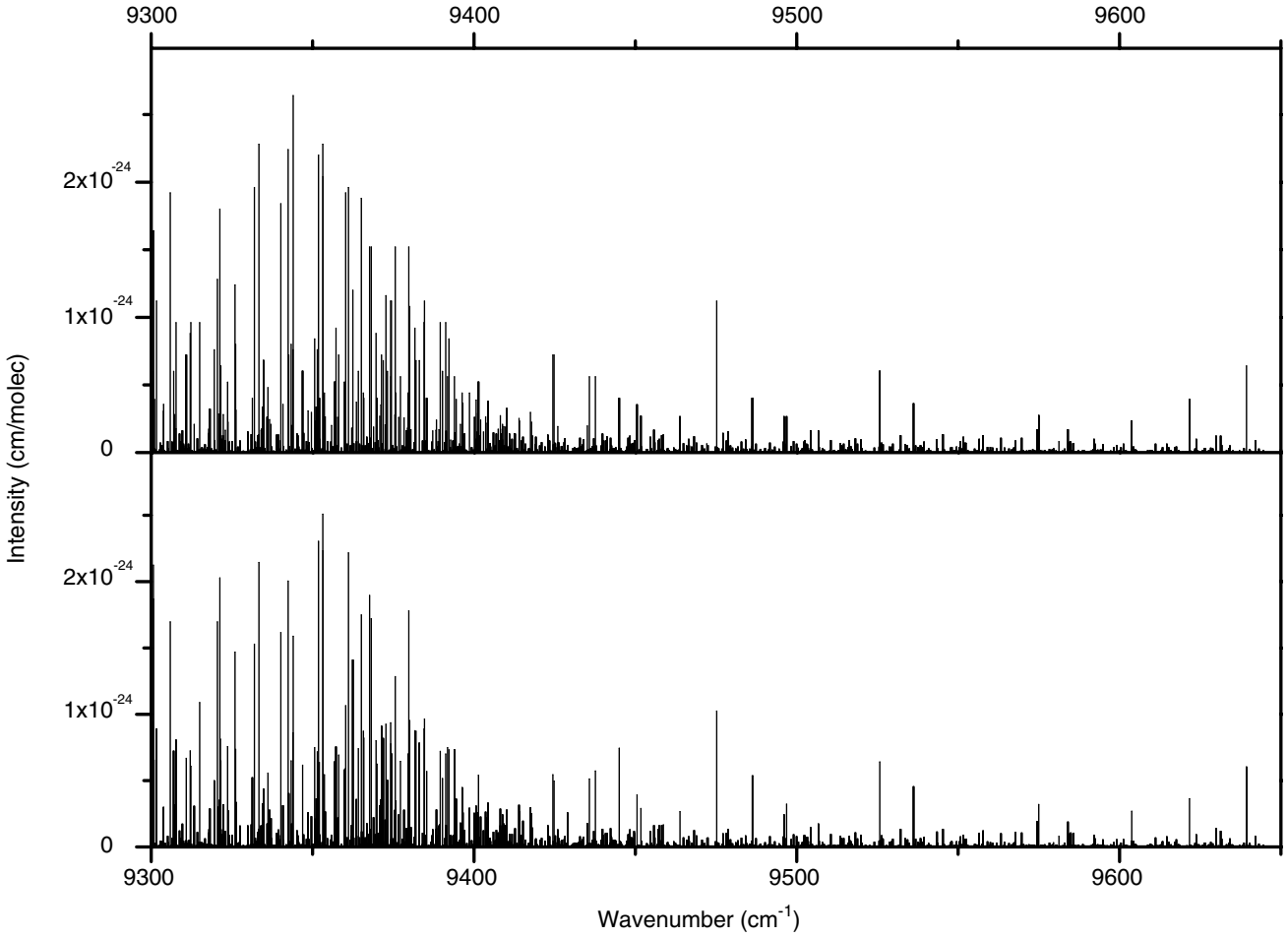

Fig. 4. Illustration of the observed and calculated intensity matching achieved in the 9100–9500 cm^{-1} region after scaling the ICLAS-VeCSEL line intensities. The upper panel represents SP calculations [21,22] for pure HDO limited to the assigned lines. The experimental stick spectrum is shown on the lower panel.

of [21,22] which consisted in the diagonalization of the matrix of the complete rovibrational Hamiltonian, and did not involve the concept of resonance interactions which is one of corner-stones in the effective Hamiltonian approach. However, for a deeper understanding of the intramolecular dynamics and a reliable rovibrational labelling, the resonance interactions between the analyzed states have to be considered. Indeed, large distortions of the calculated intensities [22] have been evidenced (see for instance [11]) and showed to be frequently connected with strong resonance perturbations of the corresponding upper levels. We present hereafter a short discussion of the possible resonance interactions between the considered vibrational states and their influence on the observed line positions and intensities. It is based on the usual general principles of resonance interactions: close values of the energy levels of the resonating states, proportionality of the intensities of transitions originating from the same lower state and involving coupled upper levels, as well as some extrapolation of the value of the matrix element of the resonance operator. In particular, this coupling term is believed to increase quickly when a highly excited bending state is involved in the resonance [26].

Transitions reaching the (041), (230), (150), and (070) upper states are due to a strong resonance link with the more intense (201)–(000), (121)–(000) and (310)–(000) bands. However, intensity borrowing seems to account for only a part of the strengthening of the transitions of the first two bands, (230)–(000) and (041)–(000). In addition, these bands seem to have, on their own, a small transition moment while the other two bands—(150)–(000) and (070)–(000), really have a resonance origin. The (150)–(000) band steals its intensity via a distant resonance interaction with the (230)–(000) band. The interaction seems to be so strong, that it leads to nearly equal transition intensities for both bands. Interestingly, the observation of the (070)–(000) band arises from resonance coupling with three vibrational bands depending on K_a values: (041)–(000) (for $K_a = 0$ levels), (121)–(000) (for $K_a = 1$ levels), and (310)–(000) (for $K_a = 2$ levels). Three lines belonging to the $6\nu_2$ and $8\nu_2$ bands were also observed due to a resonance link with the much stronger (121)–(000) and (111)–(000) bands, respectively. Such interactions have a local character and are caused by abnormal centrifugal distortion effect displayed by the HDO molecule [2,26].

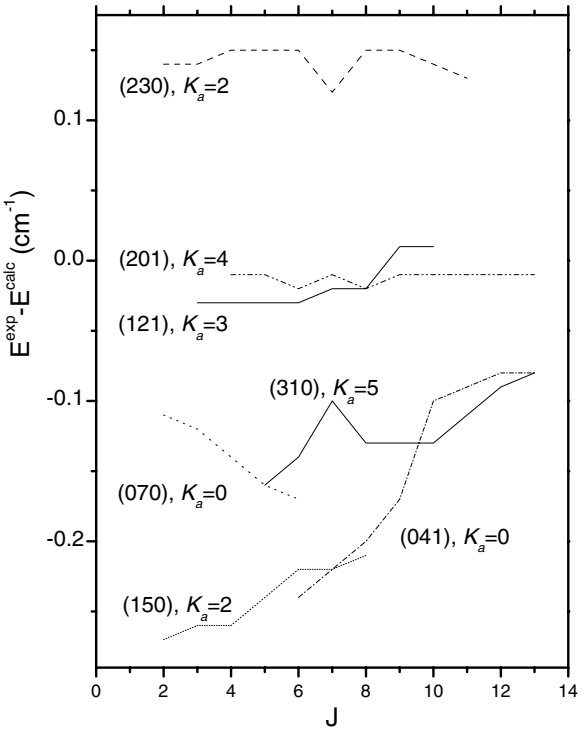

Fig. 5. Variation of the difference between the experimental and calculated [21,22] energy levels versus J, for the $K_a = 0$, 2–5 energy sublevels of seven of the analyzed vibrational states.

As stressed in [6], SP rovibrational assignments for the (230) and (150) states are often ambiguous. The new information on the experimental energy levels derived in this study and in [7] confirms this observation. In particular, for the (230) state, the energy in the J-multiplet does not increase with K_a increasing from 1 to 2 as expected (see Table 3). We attempted a rough fitting within the effective Hamiltonian approach to relabel the energy levels of the (150) and (230) states considering them as isolated, but the results were not satisfactory. Further analysis is then required to solve this problem.

Fifty four energy levels of the (310), (150), and (230) states were derived in our previous ICLAS-VeCSEL study above 9620 cm^{-1} [6]; half of them were also determined in the present work from transitions falling in our spectral region. On the other hand, additional levels of the (201) and (041) states were obtained in [7] from the FTS spectrum below 9100 cm^{-1}. For completeness, we have gathered in Tables 2 and 3, our energy levels set to those of [6,7] to provide the most complete set available for the rotational energy levels of the (201), (121), (310), (150), (230), (041), and (070) states of the HDO molecule.

4. Conclusion

The analysis of the high resolution ICLAS-VeCSEL absorption spectrum of HDO in the 9100–9640 cm^{-1} spectral region has resulted in a complete assignment of the observed transitions and the derivation of 300 new accurate energy levels for the (201), (310), (121), (041), (230), (070), and (150), states. The spectrum analysis

Table 1
Summary of the information obtained from the ICLAS-VeCSEL spectrum of HDO recorded between 9100 and 9640 cm^{-1}

VIB	E_v [a] (cm^{-1})	This work			Ref. [7]			New levels
		N levels	J_{max}	$K_{a\,max}$	N levels	J_{max}	$K_{a\,max}$	
060	7914.317[b]	1						1
012	8611.102[c]	2						2
041	9032.11[d]	102	13	7	23	8	4	82
201	9047.068	128	13	9	117	13	7	25
070	9086.32[d]	55	12	3	24	7	2	31
121	9155.817	108	15	6	62	9	6	47
150	9381.792	52	13	4	19	6	2	29
310	9292.999	148	16	8	101	14	6	42
230	9487.915	80	12	5	29	7	2	36
102	9967.023[e]	51						4
080	10119.36[g]	1						1
022	9934.789[e]	15						
003	10631.683[f]	3						
	Total	746			375			300

The count of the newly observed levels considers not only the results of [7] but also the levels determined in [6,8] thus reducing the number of newly observed levels.

[a] Vibrational term value.
[b] Experimental value from [28], see also this reference for additional levels of the (060) state.
[c] Experimental value from [27], see also this reference for additional levels of the (012) state.
[d] Extrapolated value (see text).
[e] Experimental value from [6], see also this reference for additional levels of the (102) and (022) states.
[f] Experimental value from [8], see also this reference for additional levels of the (003) state.
[g] Predicted value [21,22].

Table 2
The rotational energy levels (cm^{-1}) of the (201), (310), (121), and (041) vibrational states of HDO

J	K_a	K_c	(201)			(310)			(121)			(041)		
			$E_{obs.}$ (cm^{-1})	σ	N	$E_{obs.}$ (cm^{-1})	σ	N	$E_{obs.}$ (cm^{-1})	σ	N	$E_{obs.}$ (cm^{-1})	σ	N
0	0	0	9047.0685 F		1	9292.9990	4.1	2	9155.8178		1			
1	0	1	9062.0176 F	2.0	2	9307.6928	1.6	4	9170.9846	0.1	2			
1	1	1	9071.2899 F	2.1	3	9323.6485	1.7	3	9192.5683	1.9	2	9089.1683 F	1.7	2
1	1	0	9074.0407 F	0.2	2	9326.3668	1.5	4	9195.9426	0.4	2	9092.9770 F	0.2	2
2	0	2	9091.5837 F	0.9	3	9336.7493	1.2	5	9200.9026	0.8	3			
2	1	2	9098.4456 F	2.5	4	9350.3025	0.5	6	9220.0797	0.4	3	9116.2352		1
2	1	1	9106.6215 F	0.5	2	9358.4445	0.6	3	9230.2071	0.1	2	9127.3949 F		1
2	2	1	9147.6299		1	9406.7343	0.6	4	9279.7419	0.5	3			
2	2	0	9147.9722		1	9406.9955	0.9	4	9280.1068		1			
3	0	3	9135.1428 F	0.2	3	9379.5466	1.5	5	9245.9435	0.2	2			
3	1	3	9139.0860 F	1.8	4	9390.0867	1.1	5	9261.1886	0.3	3	9156.9572		1
3	1	2	9155.1470 F	0.3	4	9406.3227	1.5	7	9281.4242	0.4	3	9178.8294 F	0.2	2
3	2	2	9192.1581		1	9451.5263	1.6	6	9325.9035	2.7	3	9245.7607		1
3	2	1	9193.8613		1	9452.6213	2.5	10	9327.6868	0.9	5	9250.0222	0.7	2
3	3	1	9264.7774	0.3	2	9533.7042	1.8	5	9428.6242	0.5	3	9362.2007		1
3	3	0	9264.8070	0.2	2	9533.7276	1.7	4	9428.6360	0.8	2	9362.2373		1
4	0	4	9193.8324		1	9435.2967	0.7	6	9304.2833		1			
4	1	4	9191.3230		1	9442.7954	1.6	5	9316.5063	0.4	3	9211.1067		1
4	1	3	9219.2030		1	9469.6924	0.7	7	9349.3993		1	9246.9491		1
4	2	3	9251.2636		1	9506.0183	1.6	6	9387.1639	0.6	2			
4	2	2	9256.1015		1	9514.3249	2.0	5	9392.2757	2.7	3	9313.2991	0.8	3
4	3	2	9324.6354	1.6	2	9592.8133	1.2	6	9490.9132	0.1	2	9424.3165		1
4	3	1	9324.8400	2.9	3	9592.9811	1.0	7	9491.0887	3.6	3	9424.5038	1.4	2
4	4	1	9423.9760	3.2	2	9708.2114	1.8	2	9565.7043		1	9641.8567	0.6	2
4	4	0	9423.9702		1	9708.2125	1.7	3	9565.7025		1	9641.8589	3.2	2
5	0	5	9252.7416		1	9503.2876	1.7	4	9374.9274		1			1
5	1	5	9258.4274	1.0	2	9508.2123	1.6	7	9382.7224	0.1	2	9278.4454	3.5	2
5	1	4	9298.2655 F	0.2	3	9548.0786	0.9	6	9417.5546	3.3	2	9331.3790		1
5	2	4	9324.5755		1	9579.5172	1.4	5	9463.3086	1.4	2	9383.6227		1
5	2	3	9335.0496		1	9591.4824	0.7	7	9474.3704	1.8	3	9396.9477	0.9	2
5	3	3	9399.5796	0.5	3	9666.8128	2.1	7	9568.9376	3.2	2	9502.0199	0.7	2
5	3	2	9400.3532		1	9667.5532	0.8	8	9569.6212	1.0	3	9502.7995		1
5	4	2	9498.6289	2.0	2	9781.8794	1.3	3	9642.6558		1	9720.2235	0.4	3
5	4	1	9498.6458	0.5	2	9781.8908	4.5	6	9642.6678		1	9720.2907	1.5	3
5	5	1	9624.6751	3.0	2	9928.0381	0.8	3	9806.4131		1	9916.2354	1.6	2
5	5	0	9624.6764		1	9928.0378	1.4	3	9806.4130		1	9916.2344	2.4	2
6	0	6	9334.6501		1	9583.0555	1.6	4	9457.5073	0.8	2			
6	1	6	9337.6816	0.1	2	9586.0984	1.1	4	9463.3508		1	9358.7026	1.0	2
6	1	5	9391.5671 F	0.7	4	9640.8360	0.8	5	9516.8873	0.4	2			
6	2	5	9411.9470	1.2	2	9666.3475	0.5	8	9554.2059	1.0	2	9474.6785		1
6	2	4	9430.6868		1	9684.0457	1.0	8	9574.0444	2.1	2	9497.2284	0.8	2
6	3	4	9489.4917	0.0	2	9755.6753	1.0	7	9662.6275	2.7	3	9595.3971	2.0	3
6	3	3	9491.7740		1	9757.4485	0.5	5	9664.6434	0.7	2	9597.5801		1
6	4	3	9588.3528	3.8	2	9870.4510	1.8	5	9735.1513		1	9814.2756	2.2	3
6	4	2	9588.4416	1.6	2	9870.5101	1.0	3	9735.2404		1	9814.5579	0.5	2
6	5	2	9713.9218		1	10016.4472	1.0	4	9898.1716	0.1	2	10010.0194	1.4	5
6	5	1	9713.9201	1.3	2	10016.4461	0.5	3	9898.1712	0.6	2	10010.0210	1.9	5
6	6	1	9865.8744		1	10190.9359	0.4	4	10087.2944		1	10243.0112		1
6	6	0	9865.8753		1	10190.9361	0.2	4	10087.2946		1	10243.0113		1
7	0	7	9427.7878	1.1	2	9674.4796	1.3	4	9551.8569	1.7	2	9443.6696	2.3	2
7	1	7	9429.3296	3.1	2	9676.2636	0.7	5	9556.8025	0.5	2	9451.6103	2.3	2
7	1	6	9498.2325		1	9747.1519	1.5	5	9629.9893		1	9545.6195		1
7	2	6	9512.9676		1	9766.5554	1.4	7	9660.6375	1.4	3	9579.9378		1
7	2	5	9542.6084		1	9794.7964	2.0	5	9690.9683		1	9615.1356		1
7	3	5	9594.3109	2.2	3	9859.3080	1.3	6	9771.2691	1.0	2	9704.2626	3.7	2
7	3	4	9599.6392		1	9863.5949	1.2	7	9776.6368	8.0	2	9709.4527		1
7	4	4	9693.2225	1.4	3	9973.9777	0.3	3	9843.2605		1	9926.0724	1.5	4
7	4	3	9693.5369	0.8	2	9974.2038	0.8	5	9843.5863		1	9924.8269	2.3	4
7	5	3	9818.1467		1	10117.3151	0.6	3	10005.3434		1	10121.8906		1

For completeness, the set of levels presently derived from the analysis of the ICLAS-VeCSEL spectrum between 9100 and 9640 cm^{-1}, has been completed with the levels determined in [6,7] which are marked by "*I*" and "*F*," respectively. "*T*" marks tentative assignments.

Note. N is the number of lines used for the upper energy level determination and σ denotes the corresponding experimental uncertainty in 10^{-3} cm^{-1} units.

Table 2 (*continued*)

J	K_a	K_c	(201)			(310)			(121)			(041)		
			$E_{obs.}$ (cm^{-1})	σ	N	$E_{obs.}$ (cm^{-1})	σ	N	$E_{obs.}$ (cm^{-1})	σ	N	$E_{obs.}$ (cm^{-1})	σ	N
7	5	2	9818.1512	2.8	2	10117.3185	1.3	3	10005.3444		1	10121.9045		1
7	6	2	9969.5346	2.0	2	10293.1849	1.7	3	10193.8356		1	10352.5267	0.7	2
7	6	1	9969.5377	1.9	2	10293.1835	1.9	2	10193.8355		1	10352.5266	0.7	2
7	7	1	10146.5781		1	10496.5371	2.4	2				10614.6420		1
7	7	0	10146.5783		1	10496.5371	2.5	2				10614.6419		1
8	0	8	9532.5171	0.3	2	9777.5848	0.5	4	9658.0393		1	9551.4810	0.9	2
8	1	8	9533.2711		1	9778.6148	1.5	4	9663.0145	1.1	2	9556.9586	2.9	2
8	1	7	9617.3799	0.2	2	9866.1577	1.4	4	9755.8332	1.7	2	9673.4345 T		1
8	2	7	9627.3033	1.2	2	9879.9609	2.0	5	9774.6093		1	9699.0179		1
8	2	6	9670.1260		1	9921.5088	1.2	4	9823.9429		1	9749.9718	3.5	2
8	3	6	9713.7881	2.2	3	9977.5427	2.1	3	9828.9002	0.4	2	9898.0052	1.7	3
8	3	5	9724.4078	1.1	2	9986.3026	1.3	6	9838.9014		1	9905.7372	0.4	2
8	4	5	9813.2396	1.9	2	10092.5126	1.1	6				10051.2732	2.0	2
8	4	4	9814.1603	5.6	3	10093.1882	0.5	4	9967.8973		1	10051.2472		1
8	5	4	9937.4159	0.2	2	10235.8036	1.5	4	10127.9831		1	10246.7403		1
8	5	3	9937.4560		1	10235.8256	2.2	4	10128.0168		1	10246.8026		1
8	6	3	10088.0622	3.1	2	10410.1107	2.6	3	10315.6277		1	10477.5519	4.0	2
8	6	2	10088.0889		1	10410.1090	2.3	3	10315.6812 T		1	10477.5517	4.3	2
8	7	2	10264.5346	0.1	2	10612.7732	1.4	2				10739.3534		1
8	7	1	10264.5348	0.4	2	10612.7734	1.2	2				10739.3533		1
8	8	1	10465.6547		1	10842.907 I								
8	8	0	10465.6546		1	10842.907 I								
9	0	9	9649.0649	3.8	2	9892.2925	1.1	4	9781.9169	2.4	2	9670.8412	4.7	2
9	1	9	9649.4134		1	9892.9841	1.0	3	9776.2436		1	9674.5877		1
9	1	8	9748.3703	0.2	2	9997.1540	1.4	4	9893.7399	2.7	2	9813.5459	2.6	2
9	2	8	9754.6287	0.6	2	10006.2728	0.9	4	9907.3425	0.9	2	9831.5195		1
9	2	7	9812.4321 F	0.1	2	10063.2438	2.7	4	9974.6347		1			
9	3	7	9847.6138	1.5	3	10110.4460	1.6	4	9966.2887		1	10037.5832	1.1	2
9	3	6	9866.2492		1	10125.8876	0.9	5	9986.2156	1.3	2	10057.1847	0.7	2
9	4	6	9948.3869	0.1	2	10226.0552	1.4	3	10106.3077		1			
9	4	5	9950.6521		1	10227.4641	2.1	3	10108.2221	0.4	2	10194.0448		1
9	5	5	10071.7766	0.1	2	10368.4964	1.2	3				10388.0464		1
9	5	4	10071.9027	0.6	2	10368.5697	2.6	4				10388.2089		1
9	6	4	10221.4709	0.1	2	10541.7167	5.2	2	10452.7307		1	10618.0715	0.4	2
9	6	3	10221.5129	2.7	2	10541.7251	2.6	2	10452.7311		1	10618.0706	0.8	2
9	7	3	10397.2728		1	10743.5736		1				10879.5670		1
9	7	2	10397.2724		1	10743.5732		1				10879.5675		1
9	8	2	10597.6595		1	10972.8918		1						
9	8	1	10597.6594		1	10972.8918		1						
9	9	1	10822.0073		1	11228.627 I								
9	9	0	10822.0073		1	11228.627 I								
10	0	10	9777.5433	0.3	2	10018.9201	0.5	2	9913.4944	0.1	2	9804.3859	1.8	2
10	1	10	9777.6966		1	10019.3160	0.6	2	9906.6539		1	9801.7986	0.4	2
10	1	9	9890.9099	1.7	2	10139.3296	3.8	4	10043.3729	0.0	2			
10	2	9	9894.6437	0.1	2	10145.1424	1.7	3	10052.7513	1.2	2			
10	2	8	9968.5718	1.7	2	10219.1324	1.5	3	10141.0605		1	10066.6736		1
10	3	8	9995.4224	4.3	2	10256.5472	0.7	3	10119.5256	3.3	2	10192.3391	0.5	2
10	3	7	10024.9010		1	10282.2571	9.4	4	10151.6593		1	10221.4493		1
10	4	7	10098.5344	0.6	2	10374.5638	3.1	3	10261.1314		1	10350.5273		1
10	4	6	10103.4619		1	10377.9165	2.0	3				10353.5140		1
10	5	6	10221.2502	3.8	2	10515.9781	7.6	3				10545.2257		1
10	5	5	10221.7350	1.7	2	10516.2025	1.9	2				10545.6791		1
10	6	5	10369.7982		1	10688.0510	6.2	2						
10	6	4	10369.9268	0.7	2	10688.0560	9.1	2						
10	7	4				10888.9528	0.0	2				11035.2405 T		1
10	7	3				10888.9516	1.1	2				11035.2400 T		1
10	8	3	10744.3271		1									
10	8	2	10744.3276		1									
10	9	2	10967.8050		1	11372.115 I								
10	9	1	10967.8050		1	11372.115 I								
11	0	11	9917.9891	1.2	2	10157.3057		1	10038.7763 T		1	9946.3561	1.7	2
11	1	11	9918.0497	5.3	2	10158.2477	1.2	3	10049.4419		1	9944.5253	2.5	2
11	1	10	10044.9693		1	10293.4186	1.3	3	10204.6532		1			

(*continued on next page*)

Table 2 (*continued*)

J	K_a	K_c	(201)			(310)			(121)			(041)		
			$E_{obs.}$ (cm^{-1})	σ	N	$E_{obs.}$ (cm^{-1})	σ	N	$E_{obs.}$ (cm^{-1})	σ	N	$E_{obs.}$ (cm^{-1})	σ	N
11	2	10	10047.1120		1	10296.5093		1	10210.9097		1			
11	2	9	10137.4945 F	3.6	2	10388.2439	0.1	2						
11	3	9	10156.1289	0.9	2	10416.7604	1.3	2				10361.3411		1
11	3	8	10199.7166		1	10453.6368		1				10404.4249		1
11	4	8	10263.4875		1	10538.0124	3.8	2	10431.1683		1	10523.4618		1
11	4	7	10273.0769	1.6	2	10544.7150	0.4	2	10441.9200 T		1			
11	5	7	10385.8385		1	10678.3661	2.8	2						
11	5	6	10386.7495		1	10678.8866		1						
11	6	6				10849.1331	1.6	2						
11	6	5	10533.3612		1	10849.1453		1						
11	8	4				11276.210 I								
11	8	3				11276.210 I								
12	0	12	10070.4538		1	10307.2676	1.0	2	10194.0031		1	10100.0195		1
12	1	12	10070.4170		1	10307.4898	0.8	2	10204.9407		1	10098.7210		1
12	1	11	10210.7276		1	10457.4431		1	10377.6431	8.8	2			
12	2	11				10460.0634		1	10381.7385		1			
12	2	10	10318.5330		1	10569.6364		1				10510.2373		1
12	3	10	10331.5973		1	10590.3320		1				10550.4491 T		1
12	3	9				10644.5148	3.5	2				10603.6325		1
12	4	9	10442.8973		1				10616.3086		1	10709.9548		1
12	4	8				10729.1103		1				10722.8668		1
12	5	8				10855.6439		1						
12	5	7	10567.5727		1	10856.8899	1.9	2						
12	6	6	10711.7789 T		1									
13	0	13	10234.8620		1	10469.2212		1	10361.1065		1	10265.9409		1
13	1	13	10234.8143		1	10469.3797		1						
13	1	12	10388.0341		1	10633.9669 F		1						
13	2	12							10565.0840		1			
13	2	11	10510.6561		1	10762.5556		1						
13	3	10				10847.9173		1				10824.4867 T		1
13	4	9	10663.8977		1	10926.8996 T	3.3	2						
13	5	9				11047.7526 T		1						
13	5	8				11050.4939		1						
14	0	14				10642.8914		1	10539.8006		1			
14	1	14				10643.0441		1						
14	2	13				10822.5678 T		1						
15	0	15				10828.3059		1						
15	1	15							10728.3904 T		1			
15	1	14				11021.2071		1						
15	2	14				11021.7412 T		1						
16	0	16				11025.3136		1						

relied greatly on SP predictions, in particular on the quantitative matching of the observed and calculated line intensities. An unexpected high number (55) of rotational energy levels of the highly excited bending (070) state could be derived as a consequence of a strong resonance strengthening of the $7\nu_2$ band. This confirms that centrifugal distortion effect in HDO is abnormally strong and leads to considerable perturbation of its rovibrational spectrum at a high excitation of bending vibration [2,26].

No HDO transitions are presently available in the HITRAN database in the considered spectral region, thus the experimental information provided in this work makes a marked improvement into the knowledge of the HDO absorption spectrum. In particular, the generated line list may be helpful for discriminating between weak HDO lines and trace species absorption in the 9100–9640 cm^{-1} transparency region.

Acknowledgments

The expert help of E. Bertseva (Grenoble) during the ICLAS-VeCSEL recordings is warmly acknowledged. This work is jointly supported by CNRS in the frame of the ''Programme National de Chimie Atmosphérique,'' by the INTAS foundation (Project 03-51-3394) as well as a collaborative project between CNRS and RFBR (PICS Grant No. 05-05-22001). This research takes part in an effort by a Task Group of the International Union of Pure and Applied Chemistry (IUPAC, Project No. 2004-035-1-100) to compile, determine, and validate, both experimentally and theoretically, accurate frequency, energy level, line intensity, line width, and pressure effect spectral parameters of all major isotopologues of water. This work has been performed in the frame of the European research network QUASAAR (MRTN-CT-2004-512202). S.-M. Hu

Table 3
The rotational energy levels (cm^{-1}) of the (230), (070), and (150) vibrational states of HDO

J	K_a	K_c	(230)			(070)			(150)		
			$E_{obs.}$ (cm^{-1})	σ	N	$E_{obs.}$ (cm^{-1})	σ	N	$E_{obs.}$ (cm^{-1})	σ	N
0	0	0	9487.9156		1				9381.7921	1.0	2
1	0	1	9503.2835	1.2	4				9397.0303	1.0	2
1	1	1	9528.8008	2.2	4	9174.2609	1.8	2	9427.9568	0.2	3
1	1	0	9532.0413	0.8	3	9177.7155	1.8	2	9431.4219	1.6	3
2	0	2	9533.6490	1.0	4	9133.3657		1	9427.2931	1.3	3
2	1	2	9556.3596	0.6	4	9203.8195	1.2	4	9454.9554	0.3	3
2	1	1	9566.0735	1.4	3	9212.7616	1.4	3	9465.3384	3.3	3
2	2	1	9549.3421	1.3	4	9399.1347	1.8	2	9645.4923	0.8	2
2	2	0	9549.6927	2.2	3	9399.2591	0.7	4	9645.7522	6.5	4
3	0	3	9578.3410	1.8	5	9179.1221		1	9472.1203	0.4	3
3	1	3	9597.5547	1.2	5	9240.8737	0.1	2	9495.2707	1.8	4
3	1	2	9616.9051	2.9	4	9264.7087	1.4	3	9515.9703	1.1	5
3	2	2	9594.8784	3.8	6	9445.5663	1.4	6	9691.9465	1.1	4
3	2	1	9596.5320	2.4	4	9446.3482	1.4	4	9693.2713	1.5	4
3	3	1	9735.4903		1	9682.3587	2.7	2	9842.5387		1
3	3	0	9735.5095		1	9682.3607		1	9842.5537	0.4	2
4	0	4	9636.6233	1.2	4	9238.7725		1	9531.1106	1.8	5
4	1	4	9651.9966	2.5	5	9295.8320	0.9	2	9548.7055	1.6	5
4	1	3	9684.2212	1.2	5	9333.1813	0.4	2	9582.9911	0.8	4
4	2	3	9655.3407	0.3	4	9512.2502	1.8	7	9753.6437	3.8	5
4	2	2	9660.1148	2.7	5	9509.1344	1.4	8	9757.5040	6.8	2
4	3	2	9797.3540	1.7	4	9744.3360	2.8	2	9905.4627		1
4	3	1	9797.4674	1.0	3	9744.4298	2.7	3	9905.5301	0.4	2
4	4	1	9928.6481	2.8	4				10037.1799 T		1
4	4	0	9928.6528	4.5	3				10037.1782 T		1
5	0	5	9707.8820	0.4	3	9311.8475		1	9604.7898	1.8	4
5	1	5	9719.6464	2.1	4	9363.8575	0.8	2	9615.0467	1.1	3
5	1	4	9767.6088	1.1	4	9433.9199	0.2	2	9665.8424	1.4	9
5	2	4	9730.5456	1.2	3	9589.5115	0.3	4	9830.3904	1.3	3
5	2	3	9740.6111	1.0	4	9587.5678	2.2	6	9838.9880	2.7	2
5	3	3	9874.7981	4.3	2	9821.8093	1.7	3	9984.153 I		
5	3	2	9875.2208	0.5	2	9822.1677	2.0	2	9984.467 I		
5	4	2	10004.3031	4.3	2						
5	4	1	10004.2968	3.9	3						
5	5	1	10195.0767		1						
5	5	0	10195.0766		1						
6	0	6	9791.6291	0.9	3	9398.1472		1	9677.7722	1.1	4
6	1	6	9800.2387	0.0	2	9444.8721	0.5	2	9694.0639	0.2	3
6	1	5	9866.4750	5.6	3	9534.6849		1	9764.2777	1.1	3
6	2	5	9820.3343	0.4	3	9682.6139	2.5	4	9921.9308		1
6	2	4	9838.2738	1.2	3	9696.7517	0.8	3	9938.0057	3.8	2
6	3	4	9967.7883	0.0	2	9914.6897	4.2	2	10078.600 I		
6	3	3	9969.0549	2.2	2	9915.7978	1.4	2			
6	4	3	10095.2157	8.5	2						
6	4	2	10095.2596	2.7	2						
6	5	2	10285.4333		1						
6	5	1	10285.4323		1						
7	0	7	9887.5450	0.5	3				9775.2560		1
7	1	7	9893.5060	2.2	3	9538.7007	0.2	2	9785.7449	0.5	2
7	1	6	9980.1225	3.7	2	9650.4604	3.0	3	9877.0264	0.2	3
7	2	6	9922.3800	2.5	5	9791.0651		1	10028.0605		1
7	2	5	9953.0546	2.3	2	9808.5496	1.3	3	10054.540 I		
7	3	5	10076.2923	1.5	2	10022.9117		1	10188.712 I		
7	3	4	10079.2542		1	10025.5715		1	10190.958 I		
7	4	4	10201.4760	7.5	2						
7	4	3	10201.6592	5.5	3						
8	0	8	9995.5424		1	9609.9425		1	9881.3728	2.8	3
8	1	8	9999.3033	3.7	2	9645.2177	1.7	2	9888.5792	0.5	2
8	1	7	10003.3587	5.4	2	9788.7495	3.7	2	10107.7002		1
8	2	7	10040.7419	1.8	2	9914.9494		1	10148.130 I		
8	2	6	10084.5880	1.8	2	9938.2804	0.4	2	10188.256 I		
8	3	6	10200.1792		1	10146.2681		1			

(*continued on next page*)

Table 3 (*continued*)

J	K_a	K_c	(230)			(070)			(150)		
			$E_{obs.}$ (cm^{-1})	σ	N	$E_{obs.}$ (cm^{-1})	σ	N	$E_{obs.}$ (cm^{-1})	σ	N
8	3	5	10206.1692		1	10152.2310		1			
8	4	5	10323.1420		1						
9	0	9	10116.1548		1				9999.8839		1
9	1	9	10117.5310		1				10004.9036	1.1	3
9	1	8	10142.3058		1	9937.1275		1	10248.530 I		
9	2	8	10171.9183	1.4	3	10049.0939		1			
9	2	7	10232.5507		1	10084.4575 T	6.3	2	10338.051 I		
9	3	7	10339.784 I								
9	3	6	10349.9668		1	10295.6178		1			
9	4	6	10460.053 I								
9	4	5	10461.421 I								
10	0	10	10239.3668		1				10127.6110	2.0	2
10	1	10	10247.9615		1	9895.4421	2.7	2	10133.1024	2.4	2
10	1	9	10293.1718		1				10402.086 I		
10	2	9	10316.2763		1				10430.324 I		
10	2	8	10395.5724		1	10256.2345		1			
10	3	7	10510.688 I								
10	4	7	10612.424 I								
11	0	11	10387.1904		1				10269.3996		1
11	1	11	10390.9422		1				10272.6298		1
11	1	10	10456.9970	2.6	2						
11	2	10	10473.7212		1						
11	4	8	10780.013 I								
12	0	12				10214.9549		1	10420.8299		1
12	1	12							10424.6029		1
12	1	11	10629.0900 T		1						
13	0	13							10585.8121		1
13	1	13							10588.5544		1
14	2	12							11312.545 I		
			(1 0 2)								
8	7	2	11137.7414		1						
8	7	1	11137.7414		1						
9	7	3	11272.7296		1						
9	7	2	11272.7288		1						
			(0 1 2)								
10	8	3	10377.1101 T		1						
10	8	2	10377.1123 T		1						
			(0 6 0)								
8	6	3	9773.8981 T		1						
			(0 8 0)								
12	0	12	10182.4731	1.1	2						

For completeness, the set of levels presently derived from the analysis of the ICLAS-VeCSEL spectrum between 9100 and 9640 cm^{-1}, has been completed with the levels determined in [6] which are marked by "*I*." "*T*" marks tentative assignments.
Note. N is the number of lines used for the upper energy level determination and σ denotes the corresponding experimental uncertainty in 10^{-3} cm^{-1} units.

(USTC, Hefei, China) is acknowledged for communicating the FTS spectrum of [7] reproduced in Fig. 3.

Appendix A. Supplementary data

Supplementary data for this article are available on ScienceDirect (www.sciencedirect.com) and as part of the Ohio State University Molecular Spectroscopy Archives (<http://msa.lib.ohio-state.edu/jmsa_hp.htm/>).

References

[1] O. Naumenko, E. Bertseva, A. Campargue, J. Mol. Spectrosc. 197 (1999) 122–132.
[2] O. Naumenko, A. Campargue, J. Mol. Spectrosc. 199 (2000) 59–72.
[3] O. Naumenko, E. Bertseva, A. Campargue, D. Schwenke, J. Mol. Spectrosc. 201 (2000) 297–309.
[4] E. Bertseva, O. Naumenko, A. Campargue, J. Mol. Spectrosc. 203 (2000) 28–36.
[5] A. Campargue, E. Bertseva, O. Naumenko, A. Campargue, J. Mol. Spectrosc. 204 (2000) 94–105.
[6] E. Bertseva, O. Naumenko, A. Campargue, J. Mol. Spectrosc. 221 (2003) 38–46.
[7] O.N. Ulenikov, S.-M. Hu, E.S. Bekhtereva, Q.-S. Zhu, J. Mol. Spectrosc. 231 (2005) 57–65.
[8] O. Naumenko, S.–M. Hu, S.–G. He, A. Campargue, Phys. Chem. Chem. Phys. 6 (2004) 910–918.
[9] M. Bach, S. Fally, P.-F. Coheur, M. Carleer, A. Jenouvrier, A.C. Vandaele, J. Mol. Spectrosc. 232 (2005) 329–338.
[10] A. Campargue, I. Vasilenko, O. Naumenko, 234 (2005) 216–227.

[11] A.D. Bykov, V.P. Lopasov, Yu.S. Makushkin, L.N. Sinitsa, O.N. Ulenikov, V.E. Zuev, J. Mol. Spectrosc. 94 (1982) 1–27.
[12] A. Garnache, A.A. Kachanov, F. Stoeckel, R. Houdré, J. Opt. Soc. Am. B. 17 (2000) 1589–1598.
[13] E. Bertseva, A.A. Kachanov, A. Campargue, Chem. Phys. Lett. 351 (2002) 18–26.
[14] Y. Ding, V.I. Perevalov, S.A. Tashkun, J.-L. Teffo, S. Hu, E. Bertseva, A. Campargue, J. Mol. Spectrosc. 220 (2003) 80–86.
[15] E. Bertseva, V. Perevalov, S.A. Tashkun, A. Campargue, J. Mol. Spectrosc. 226 (2004) 196–200.
[16] Y. Ding, E. Bertseva, A. Campargue, J. Mol. Spectrosc. 212 (2002) 219–222.
[17] Y. Ding, O. Naumenko, S. Hu, E. Bertseva, A. Campargue, J. Mol. Spectrosc. 217 (2003) 222–238.
[18] O. Naumenko, A. Campargue, J. Mol. Spectrosc. 221 (2003) 221–226.
[19] A. Garnache, A. Liu, L. Cerutti, A. Campargue, Chem. Phys. Lett. 416 (2005) 22–27.
[20] E. Bertseva, A. Campargue, Opt. Com. 232 (2004) 251–261.
[21] H. Partridge, D.W. Schwenke, J. Chem. Phys. 106 (1997) 4618–4639.
[22] D.W. Schwenke, H. Partridge, J. Chem. Phys. 113 (2000) 6592–6597.
[23] R.N. Tolchenov, J. Tennyson, S.V. Shirin, N.F. Zobov, O.L. Polyansky, A.N. Maurellis, J. Mol. Spectrosc. 221 (2003) 99–105.
[24] A. Campargue, O. Leshchishina, O. Naumenko, in preparation.
[25] R. Toth, J. Mol. Spectrosc. 162 (1993) 20–40.
[26] A. Bykov, O. Naumenko, L. Sinitsa, B. Voronin, J.-M. Flaud, C. Camy-Peyret, R. Lanquetin, J. Mol. Spectrosc. 205 (2001) 1–8.
[27] S.–M. Hu, S. He, J. Zheng, X. Wang, Y. Ding, Q. Zhu Qing-shi, Chin. Phys. 10 (2001) 1021–1037.
[28] O.V. Naumenko, S. Voronina, S.-M. Hu, J. Mol. Spectrosc. 227 (2004) 151–157.